An Effective Catalyst for the Rapid Reduction of 4-Nitrophenol to 4-Aminophenol in a Novel RGO-$ZnWO_4$-Fe_3O_4 Nanocomposite

***Nageshwar G, ** Dr. Kailas Narayan Sonune**

**Research Scholar, **Research Supervisor*

Faculty of Chemistry, OPJS University, Churu, Rajasthan

ABSTRACT

Science's amazing and fast expanding field of nanotechnology has developed. It has changed the course of history for the entire planet by opening up a variety of horizons in various fields. Nanomaterials are attractive because of their enormous surface area and very small size. In rGO/Au, rGO/Ag, rGO/Pt, and GO, the relative intensity ratios of ID/IG were 1.106, 1.078, 1.047, and 0.863, respectively. The findings demonstrated the creation of rGO and the decoration of rGO with noble metal nanoparticles. Additionally, 4-nitrophenol was used to study the developed nanocomposites' catalytic properties. The reduction of 4-nitrophenol using the catalysts. The apparent rate constant k values were used to assess the catalysts' catalytic performance.

Keywords: *Ag NPs/RGO-LS, high-efficient catalytic reduction, reusability, 4-nitrophenol, bimetallic nanoparticles*

INTRODUCTION

Every person on earth depends on water, which makes up 70% of the planet's surface and is therefore a basic requirement for existence. However, severe ecological deterioration poses a threat to human health. As a result of industrialization, environmental contamination has grown to be a significant problem in both developed and developing countries. Cleanup of contaminated water, air, and soil is a major challenge, particularly for developing countries. Heavy metal ions, inorganic compounds (nitrates, chlorides, phosphates, etc.), colors (synthetic and natural), surfactants, medicines, pesticides, and several more complex compounds are among the primary pollutants in water (including surface water, groundwater, and tap water). The main sources of heavy metals include mining, metallurgical processes, agricultural operations, and industrial effluents. Automobile discharge is a significant source of lead emission. The smelting process yields other metals like copper, zinc, and arsenic. The primary source of mercury, tin, and selenium is the burning of fossil fuels, whereas the usage of pesticides is a source of arsenic production. The manufacture of dyes, which is very closely linked to industrial processes, is a significant category of developing pollutants.

The main industries using dyes are the textile industry to color fabrics, the biochemical and biological staining industry, the food industry to improve the texture of food products, cosmetics, leather goods, paint, and pigments. The pharmaceutical industry's manufacture of a huge stock of medications for varied illnesses represents another industrial sector achievement. Contrary to the health benefits brought about by the creation of such medications, the release of certain antibiotics into the environment endangers human life. Furthermore, expired medications are also thrown out, which results in contamination and negative effects. The same reasoning holds true for the use of pesticides and surfactants, which, after being applied to the required extent, are allowed to run amok in the environment and have hazardous effects. The various pesticides, herbicides, and insecticides used to spray crops in order to increase yields frequently do not entirely disappear, making their way into the food chain and posing serious health risks. These pollutants have lately been labeled as emerging toxins that directly threaten human health and have catastrophic ecological effects.

The main targets of these toxins are people, either directly through water consumption or indirectly through the food chain. The degradation of the environment brought on by such harmful substances eventually affects people's health. Most of the time, these pollutants are known to be mutagenic and carcinogenic chemicals. Significant harm results from heavy metal pollution. For instance, cadmium, a human carcinogen, damages the lungs and may cause kidney illness and bone fragility. While chromium (VI) is extremely poisonous, chromium in the form of chromium (III) is a necessary nutrient. Asthma, cough, shortness of breath, or wheezing are some of the typical health problems linked to chromium. Lead has been shown to be the cause of a number of illnesses, including kidney and brain cell damage that can result in death. Mercury is another dangerous metal that has the potential to permanently injure important human organs. As a result, the brain begins to malfunction, which leads to irritation, behavioral changes, tremors, and impaired vision or hearing. Dyes are yet another class of hazardous pollutants that, when used excessively, can have negative effects. The azo group included in the dye's structure is linked to its toxicity, making it a complicated system. The definition of the azo group states that it has a core nitrogen-nitrogen double bond, making it electron-deficient. Such azoic dyes are particularly visible in wastewater, which affects water transparency and has an unfavorable aesthetic effect. The adverse effects of these substances on human health, which include allergies, cramping, kidney failure, liver damage, and genetic abnormalities, are the more significant element of their existence in wastewater. Pharmaceuticals fall under the group of biologically active substances created for the treatment of sickness in living things. In addition to the beneficial effects of these pharmaceutical substances, their biological activity may also negatively impact non-target creatures, hurting the ecosystem's ability to function and the ecosystem services that are related to it.

Additionally, dumping unwanted or expired medications into the environment without supervision may have detrimental effects on human health. Hormonal disturbances, infertility, and colorectal cancers are the most frequent health problems brought on by pharmaceutical pollutants. Phosphates and nitrates are other toxins that have detrimental effects on both human health and the environment. Although nitrate by itself is innocuous, its conversion into nitrite results in methemoglobinemia, which impairs hemoglobin's capacity to absorb oxygen and leads to gastrointestinal malignancies. Phosphates and nitrates in wastewater have negative environmental effects that cause eutrophication, which causes hazardous algal blooms. These problems necessitate the creation of safety precautions against these dangerous pollutants. Thus, it is imperative that contaminants be removed. The development of such methods that remove harmful contaminants with little effort and expense while producing effective outcomes has been the focus of research. reverse osmosis, chemical precipitation, membrane filtration, coagulation and flocculation, irradiation, electrochemical treatment techniques, and advanced oxidation processes are a few of the different methods used to remove pollutants from water bodies. These methods are widely used to remove harmful contaminants from wastewater bodies, but for one reason or another, their effectiveness is constrained.

Numerous aspects, such as managing productivity, operational strategy, energy requirements, and financial benefit, may have an impact on how these tactics are applied. Researchers are now focusing on sportive and photocatalytic methods in their attempt to create a method that offers improved contamination removal. Both sorption and photocatalytic procedures have made it possible to completely remove contaminants, and several studies in the literature support the efficacy of both methods in removing contaminants (Figure 1). Nanomaterials (NMs) are currently replacing the traditional materials that have been employed up to now for the sorption and photocatalysis of pollutants because of their novel and effective methodology. This review highlights the significance of functionalized nanomaterials (FNMs) in the modern era by compiling examples of their most cutting-edge and creative applications in environmental remediation.

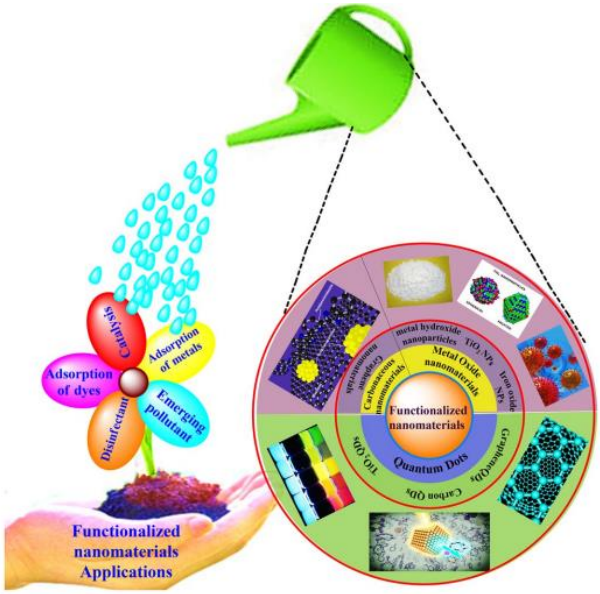

Figure 1:- Possible applications of covalent/non-covalent functionalized nanomaterials

LITERATURE REVIEW

Mohamed Jaffer Sadiq M (2016) The manufacture of a novel reduced graphene oxide-zinc tungstate-iron oxide (RGO-$ZnWO_4$-Fe_3O_4) nanocomposite using a one-pot microwave process is described here, along with information on the catalyst's effectiveness in reducing 4-nitrophenol (4-NP) to 4-aminophenol (4-AP) using sodium borohydride ($NaBH_4$). X-ray diffraction (XRD), field emission scanning electron microscopy (FESEM), transmission electron microscopy (TEM), Fourier transformed infrared spectroscopy (FTIR), Raman spectroscopy, and X-ray photoelectron spectroscopy (XPS) methods were used to characterize the RGO-$ZnWO_4$-Fe_3O_4 nanocomposites as they had been prepared. When reducing 4-NP to 4-AP, the produced nanocomposites demonstrated remarkable catalytic performance. At room temperature, the reaction was finished in approximately 40 seconds. The RGO in the nanocomposite RGO-$ZnWO_4$-Fe_3O_4 plays a crucial part in enhancing the catalytic performance by facilitating simple electron transport and enhancing substrate adsorption on graphene sheets. In addition to its outstanding stability and reusability, the synergistic effects of RGO, $ZnWO_4$, and Fe_3O_4 in the RGO-$ZnWO_4$-Fe_3O_4 nanocomposite toward reduction make it an effective contender as catalyst for aromatic chemical hydrogenation processes in both research and industrial applications.

Xiaokun Wang (2022) Rapidly restoring highly concentrated 4-nitrophenol effluent to room temperature is still a challenging task. In this study, CuO nanoparticle-loaded ZnWO4 nanoplates were created. At the same time, their catalytic activity was looked into to see how quickly 4-nitrophenol could be removed at ambient temperature. For the quick restoration of highly concentrated 4-nitrophenol effluent, we discover that CuO nanoparticles loaded $ZnWO_4$ nanoplates have excellent catalytic activity and are recyclable. When the CuO nanoparticles loaded $ZnWO_4$ nanoplates are utilized as a catalyst, 4-nitrophenol can be virtually completely removed from the 1.0 103 mol L1 (100 mL) solution in nine minutes. Nearly eleven times as fast as Ag nanoparticles, the 4-nitrophenol reduction appears to have an apparent rate constant. Furthermore, even when NaBH4 is partially substituted by methyl alcohol, this catalyst can still display exceptional activity.

Sadiq Mohamed (2018) It is still difficult to quickly get highly concentrated 4-nitrophenol effluent to room temperature. $ZnWO_4$ nanoplates filled with CuO nanoparticles were produced for this work. Their enzymatic activity was also investigated to determine how rapidly 4-nitrophenol could be eliminated at room temperature. We find that CuO nanoparticles loaded $ZnWO_4$ nanoplates have good catalytic activity for the fast restoration of highly

concentrated 4-nitrophenol effluent and are recyclable. In nine minutes, 4-nitrophenol can be almost entirely removed from the 1.0 103 mol L1 (100 mL) solution using the CuO nanoparticle-loaded $ZnWO_4$ nanoplates as a catalyst. The 4-nitrophenol reduction appears to have an apparent rate constant, and it happens almost eleven times as quickly as Ag nanoparticles. Furthermore, this catalyst can still exhibit excellent activity even when $NaBH_4$ is only partially substituted by methyl alcohol.

Rahul Krishna (2015) Palladium-nickel boride-silica and reduced graphene oxide were successfully combined to create a nanocomposite catalyst known as Pd@NixB-SiO_2/RGO, or simply Pd@NSG. This catalyst exhibits a high catalytic performance for the conversion of 4-nitrophenol (4-NP) to 4-aminophenol (4-AP) and an improved hydrogen spillover mechanism. Several approaches were used to characterize the Pd@NSG nanocomposite's structure, chemistry, and morphology. The spillover impact on the Pd@NSG nanocomposite and its increased H2 uptake capacity (0.7 wt%) compared to SiO_2/RGO (0.05 wt%) under 50 bar pressure at RT are directly revealed by the H_2 adsorption experiment. In contrast to NixB-SiO_2/(7200 RGO's s), Pd@NSG's 4-NP reduction reaction exhibits unusually high activity (120 s) and outstanding stability up to 5 cycles. In both tests, hydrogen atoms were easily dissociated on the Pd (active sites) activator and then transported to receptor sites.

Xiang-kai Kong (2013) It has been reported that N-doped graphene (NG) can catalyze the conversion of 4-nitrophenol (Nip) to 4-aminophenol (Amp) without the use of metal. Without the creation of any byproducts, Nip might be entirely converted to Amp. The NG's activity is comparable to several of the metallic catalysts that have been previously reported. It's interesting to note that while all metallic catalysts follow pseudo-first-order kinetics, the NG sheet-catalyzed process exhibits pseudo-zero-order kinetics. The in-situ FTIR experiment proved that the O atoms in the hydroxyl groups of Nip ions will react with NG to form Nip ions. This adsorption model was supported by theoretical studies, which also indicated that the Nip ion adsorption is the crucial phase that results in the pseudo-zero-order kinetics. Additionally, the only carbon atoms on the NG surface that can be activated and act as the active sites are those adjacent to the doped N atoms. As anticipated, the catalytic reduction reaction is aided by the four different types of doped N atoms in that they all promote Nip's adsorption and activation.

MATERIALS AND METHODS

Sinopharm Chemical Reagent Co., Ltd. provided the chloroauric acid tetrahydrate ($HAuCl_{44}H_2O$), chloroplatinic acid ($H_2PtCl_{46}H_2O$), sodium borohydride ($NaBH_4$), hydrazine hydrate, 4-nitrophenol (4-NP), and silver nitrate ($AgNO_3$).

Fabrication of rGO-Supported Noble Metal Composites

Hydrazine hydrate was used as a reducing agent during the one-pot, simple process used to create the composites. GO (50 mg) and deionized water (50 mL) were ultrasonically dispersed to create a GO aqueous solution for the synthesis of rGO/noble metal nanoparticles. A chloroauric acid tetrahydrate aqueous solution was created by ultrasonically dissolving $HAuCl_{44}H_2O$ (0.5 mmol) in 10 mL of deionized water. The GO aqueous solution was transferred to a two-neck flask, where it was mechanically stirred in with the gold precursor solution. The aforementioned mixture was mechanically stirred and heated to 90 C after 5 minutes. The rGO/Au composite was then cleaned and obtained (as shown in Figure 2). The same method was used to create the rGO/Pt and rGO/Ag composites.

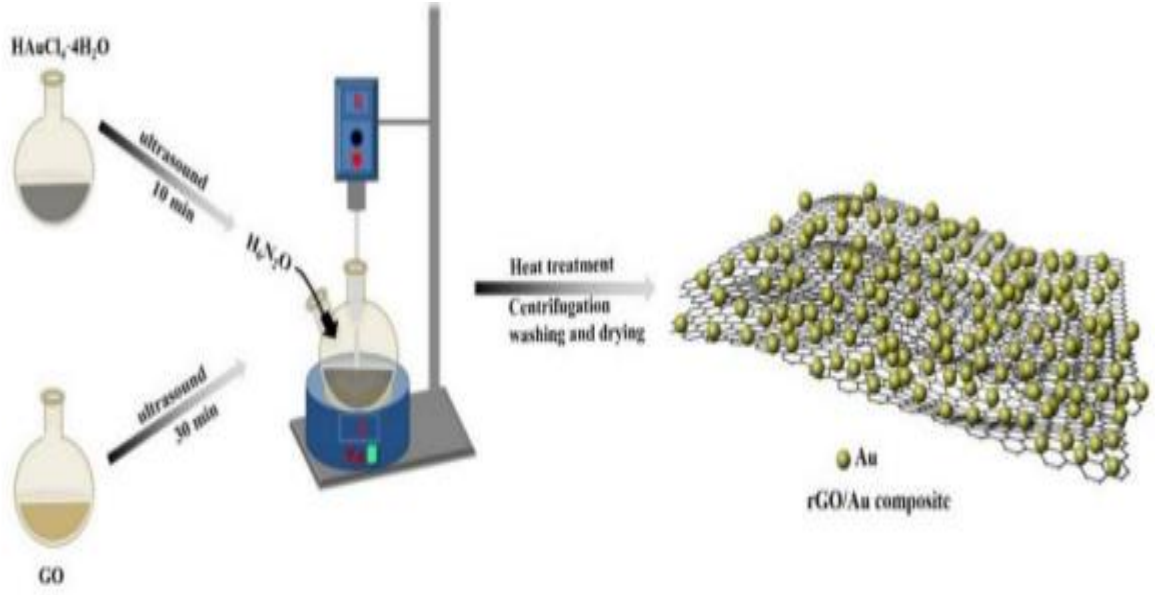

Figure 2. Schematic illustration for the synthesis of the rGO/Au composite

Applications of rGO-Supported Noble Metal Composites

The reduction of 4-nitrophenol (4-NP) with $NaBH_4$ was carried out using the rGO-supported noble metal composites. Many different types of functional nanomaterials have had their catalytic characteristics estimated using this catalytic reduction technique. With the aid of a UV-visible spectrometer, the catalytic reduction reaction process was seen. In this experiment, a conventional quartz cuvette was filled with 4-NP (0.1 mL, 0.005 M), deionized water (2 mL), and $NaBH_4$ (1 mL, 0.2 M). The mixture's distinctive peak moved from 317 nm to 400 nm, and the color immediately turned brilliant yellow, confirming the synthesis of 4-NP anions. The liquid would turn colorless when a catalyst (100 L, 2 mg/mL) was added, and the peak intensity would drop off swiftly. Additionally, the peak (at 300 nm) showed up, confirming the formation of 4-AP. The catalysts' catalytic performances were then contrasted. The Supplementary Materials provide further information in greater detail on the tools and procedures.

RESULTS AND DISCUSSION

Figure 3 depicts the image of untreated LS, alkaline-treated LS, and the hybrid Ag NPs/RGO-LS while also illuminating the three-step process used to create Ag NPs/RGO-LS. The experimental part contains the specific procedures. The UV-vis spectra of GO and $AgNO_3$/GO dispersion are displayed in Figure 3. The GO adsorption spectrum shows two distinctive peaks.

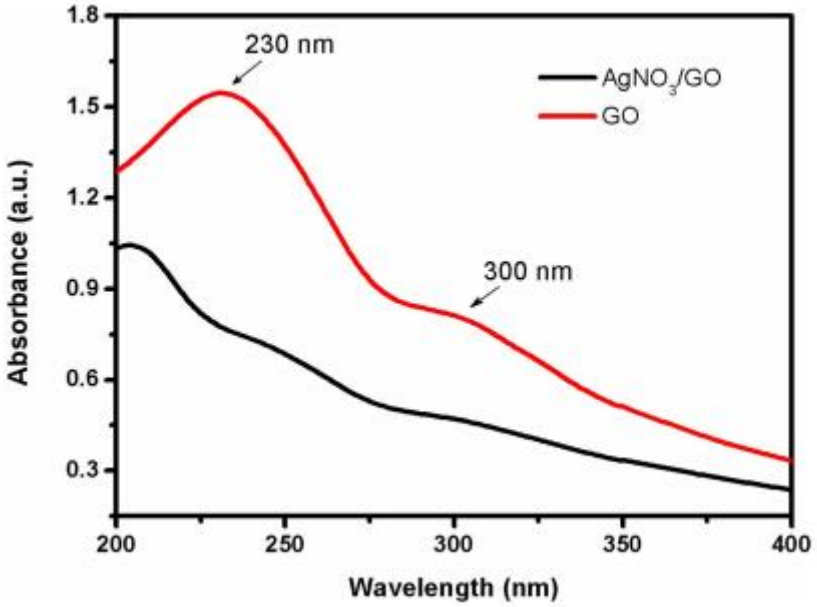

Figure 3. UV–vis spectra of GO and $AgNO_3$/GO

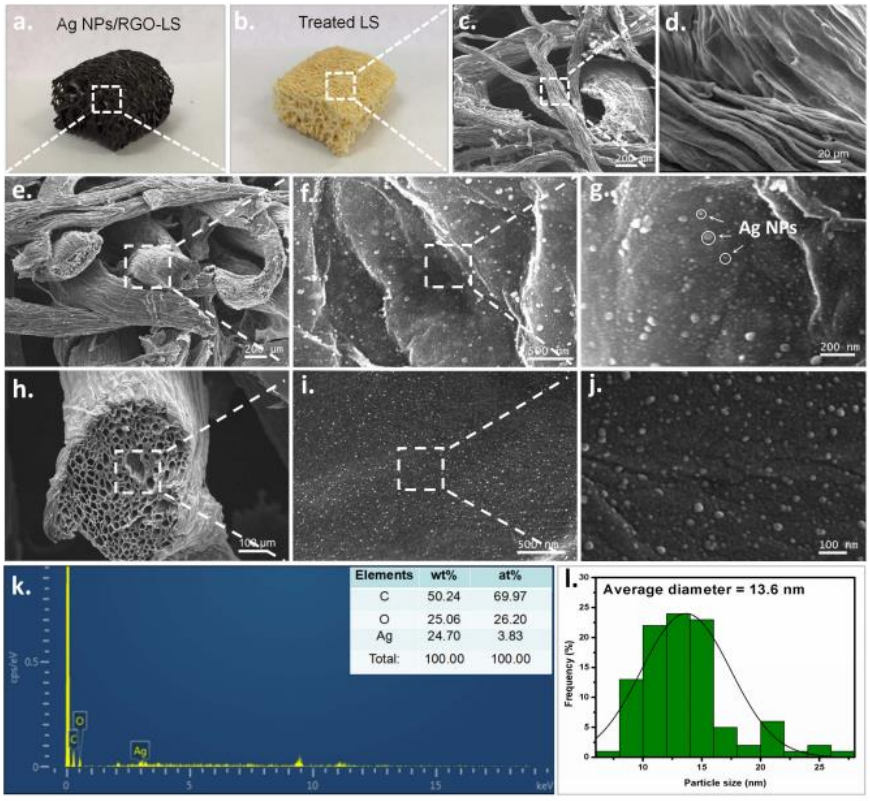

Figure 4 . (a), (b) The SEM pictures of Ag NPs/RGO-LS hybrids and treated LS. (c), (d) The surface of treated LS at high magnifications. (e)–(g) The surface of Ag NPs/RGO-LS hybrids at different magnifications. (h)–(j) The cross-section of a loofah fiber and the internal surface of fiber at high magnifications. (k) EDX spectrum of Ag NPs/RGO-LS hybrid. (l) Particle size distribution of the Ag NPs.

The transitions of the C-C and C=O bonds, respectively, are represented by the peak at 230 nm and a shoulder peak at roughly 290–300 nm. However, the two GO characteristic peaks vanished in the $AgNO_3$/GO dispersion, which could be explained by the fact that GO nanosheets were electrostatically loaded with Ag ions. Figures 4(a) and (b) show SEM images of hybrid Ag NPs/RGO-LS and alkaline-treated LS, respectively. The three-dimensional structure of LS is spontaneously created from a random matting of fibers with various morphologies and diameters, as can be seen in figure 4 (c). From the cross-section of a loofah fiber (figure 4(h)), it can be seen that the fibers have a rich internal porous structure. The surface of the treated LS is visible at high magnification in Figures 4(c) and (d). The huge surface area of processed LS is a result of the numerous grooves on the surface. Online at stacks.iop.org/NANO/29/315702, Figure S1 by media contrasts the morphologies of treated and untreated LS.

Figures 5(c) and (d) depict the untreated fibers, which have a homogenous appearance and an exterior layer that is rich in lignin. Due to the removal of surface components including lignin and hemicellulose, alkaline-treated fibers exhibit an uneven surface (figures 5(a) and (b)). The loofah fibers develop numerous irregularly spaced canals on their surface as a result of the elimination of lignin and hemicellulose, which exposes the internal structure and expands the surface area of LS. The surface of Ag NPs/RGO-LS is seen at various magnifications in Figures 5(e)–(g). Figures 5(h)–(j) depict the inside surface of a loofah fiber and its cross-section.

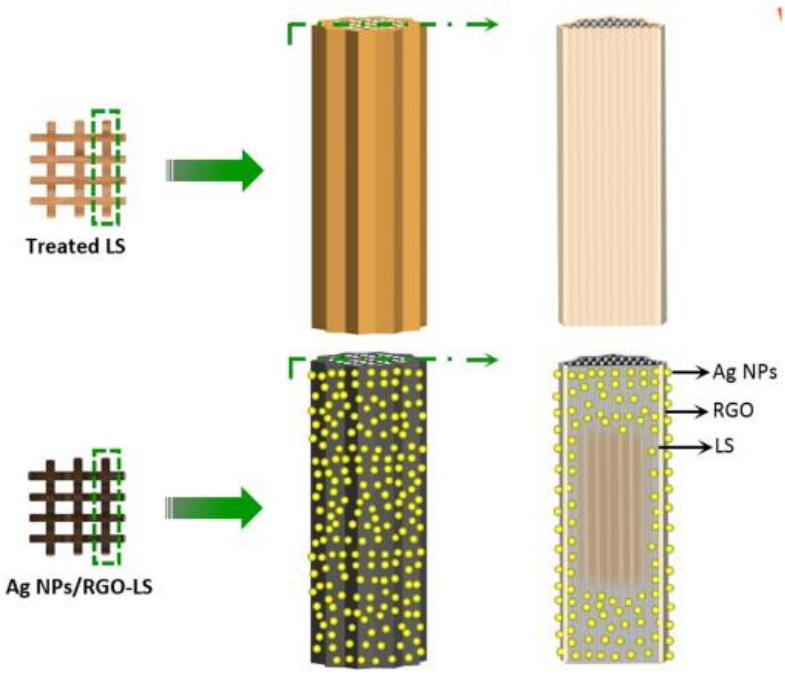

Figure 5. The distribution of RGO and Ag NPs on the LS

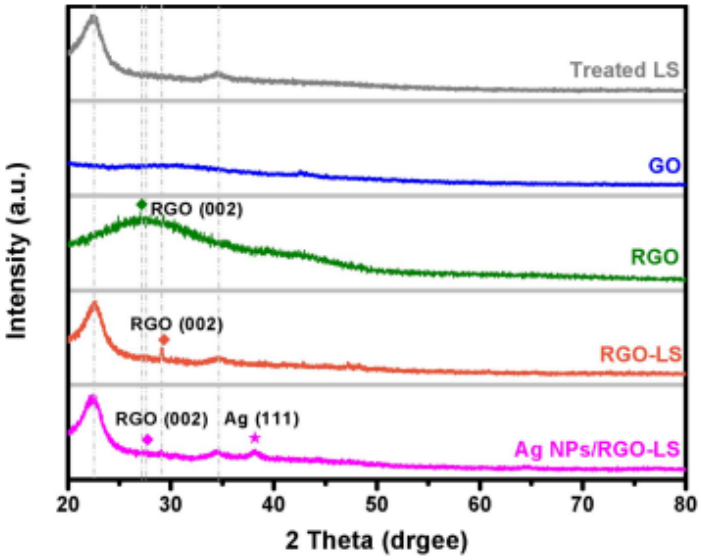

Figure 6. Typical XRD patterns of treated LS, GO, RGO, RGO-LS, and Ag NPs/RGO-LS hybrid.

Ag NPs may be shown to be uniformly dispersed throughout the fibers' internal micropores and external surface. The EDX spectrum of Ag NPs/RGO-LS is shown in Figure6, which demonstrates the existence of the components C, O, and Ag and demonstrates the absence of any other impurity elements. Ag NPs are estimated to be 24.7% in weight and 3.83% in atomic percentage, respectively, based on the distribution of the elements in the inset table of figure 6. The mean diameter of Ag NPs is 13.6 nm, and figure 6 depicts the particle size dispersion. The distribution of Ag NPs and RGO on the treated LS is shown in Figure 6. RGO and Ag NPs were dispersed across the fibers' outer surface, as seen from the front. In the interior micropores at the outside surface and the two opened ends of an Ag NPs/RGO-LS fiber, there are numerous RGO nanosheets and Ag NPs spread out. In the deepest micropores, where the Ag+/GO solution was difficult to enter, Ag NPs and RGO practically do not exist. To demonstrate that the Ag+/GO solution was unable to enter the deepest micropores. The supporting information now includes a photo of the sectional image Ag NPs/RGO-LS. Figure 6 demonstrates how the color of the deepest micropores (the LS's original color) differs noticeably from the color of the surface (the color of RGO). Where there is it, there will be black when the Ag+/GO is lowered.

CONCLUSION

Researchers have created sophisticated, quick, and precise techniques for the removal of a range of contaminants, especially those coming from industrial sources, in response to the widespread concern about wastewater contamination. These toxins have harmful effects on living things, necessitating the creation of effective decontamination techniques. In conclusion, the unique Ag NPs/RGO-LS hybrid has been created using a quick and efficient one-step reduction approach. Gold nanoparticles have a smaller crystalline size than silver and platinum nanoparticles. According to calculations, the ID/IG ratios of rGO/Au, rGO/Ag, and rGO/Pt are 1.106, 1.078, and 1.047, respectively. The rGO/Au catalyst showed the best catalytic activity for 4-NP reduction because its k value was higher than that of rGO/Ag and rGO/Pt. The smaller crystalline size of gold NPs and their distinctive structural traits may be responsible for the increased catalytic activity for rGO/Au. In the catalytic reduction of 4-NP, the Ag NPs/RGO-LS as produced demonstrated great efficiency and good reusability. This hybrid totally eliminates the Ag NPs' difficulties with agglomeration and low recovery rates. There has been discussion of the processes underlying very effective catalytic activity. Ag NPs now have a wide range of uses thanks to the findings, and the method used here can be simply applied to other metal NPs-support systems for highly effective and reusable catalysts, etc.

REFERENCE

1. Sadiq M, Mohamed Jaffer & Denthaje, Krishna. (2016). Novel RGO-$ZnWO_4$-Fe_3O_4 Nanocomposite as an Efficient Catalyst for Rapid Reduction of 4-Nitrophenol to 4-Aminophenol. Industrial & Engineering Chemistry Research. 55. 10.1021/acs.iecr.6b01882.
2. Wang, Xiaokun & Li, Xiangqing & Qin, Lixia & Zhang, Taiyang & Kang, Shi-Zhao. (2022). An efficient catalyst for rapid restoration of highly concentrated 4-nitrophenol effluent at room temperature: $ZnWO_4$ nanoplates loaded with CuO nanoparticles. Journal of Physics and Chemistry of Solids. 163. 110595. 10.1016/j.jpcs.2022.110595.
3. Sadiq Mohamed (2018) "Novel RGO-$ZnWO_4$-Fe_3O_4 Nanocomposite as an Efficient Catalyst for Rapid Reduction of 4-Nitrophenol to 4-Aminophenol [2016]" Volume: 55 Issue: 27
4. Rahul Krishna (2015) "Reduction of 4-nitrophenol to 4-aminophenol using a novel Pd@NixB–SiO_2/RGO nanocomposite: enhanced hydrogen spillover and high catalytic performance" VL-5 IS-74, http://dx.doi.org/10.1039/C5RA05523G
5. Xiang-kai Kong (2013) "Metal-free catalytic reduction of 4-nitrophenol to 4-aminophenol by N-doped graphene A1 - Kong, Xiang-kai" VL - 6, IS - 11
6. Ray, P. C. Size and Shape Dependent Second Order Nonlinear Optical Properties of Nanomaterials and Their Application in Biological and Chemical Sensing. Chem. Rev. 2010, 110, 5332.
7. Shilcrat, S. Process Safety Evaluation of a Tungsten-Catalyzed Hydrogen Peroxide Epoxidation Resulting in a Runaway Laboratory Reaction. Org. Process Res. Dev. 2011, 15, 1464.
8. Kimura, T.; Kamata, K.; Mizuno, N. A Bifunctional Tungstate Catalyst for Chemical Fixation of CO_2 at Atmospheric Pressure. Angew. Chem., Int. Ed. 2012, 51, 6700.
9. Roy, S.; Bhar, S. Sodium Tungstate-Catalyzed "on-Water" Synthesis of B-Arylvinyl Bromides. Green Chem. Lett. Rev. 2010, 3, 341
10. Wu, Y. G.; Wen, M.; Wu, Q. S.; Fang, H. Ni/Graphene Nanostructure and Its Electron-Enhanced Catalytic Action for Hydrogenation Reaction of Nitrophenol. J. Phys. Chem. C 2014, 118, 6307.
11. Moussa, S.; Siamaki, A. R.; Gupton, B. F.; El-Shall, M. S. Pd, Partially Reduced Graphene Oxide Catalysts (Pd/PRGO): Laser Synthesis of Pd Nanoparticles Supported on PRGO Nanosheets for Carbon-Carbon Cross Coupling Reactions. ACS Catal. 2012, 2, 145
12. Siamaki, A. R.; Khder, A. E. R. S. K.; Abdelsayed, V.; El-Shall, M. S.; Gupton, B. F. Microwave-Assisted Synthesis of Palladium Nanoparticles Supported on Graphene: A Highly Active and Recyclable Catalyst for Carbon-Carbon Cross-Coupling Reactions. J. Catal. 2011, 279, 1.
13. Meng, N.; Zhang, S.; Zhou, Y.; Nie, W.; Chen, P. Novel Synthesis of Silver/Reduced Graphene Oxide Nanocomposite and Its High Catalytic Activity Towards Hydrogenation of 4-Nitrophenol. RSC Adv. 2015, 5, 70968.
14. Woo, H.; Kim, J. W.; Kim, M.; Park, S.; Park, K. H. Au Nanoparticles Supported on Magnetically Separable Fe_2O_3-Graphene Oxide Hybrid Nanosheets for the Catalytic Reduction of 4- Nitrophenol. RSC Adv. 2015, 5, 7554.
15. Huang, G.; Shi, R.; Zhu, Y. Photocatalytic Activity and Photoelectric Performance Enhancement for $ZnWO_4$ by Fluorine Substitution. J. Mol. Catal. A: Chem. 2011, 348, 100.